HHS Public Access

Author manuscript

Nat Genet. Author manuscript; available in PMC 2018 August 05.

Published in final edited form as:

Nat Genet. 2018 March ; 50(3): 349–354. doi:10.1038/s41588-018-0048-5.

CLCN2 Chloride Channel Mutations in Familial Hyperaldosteronism Type II

Ute I. Scholl[1,2,*], **Gabriel Stölting**[3,#], **Julia Schewe**[1,#], **Anne Thiel**[1], **Hua Tan**[3], **Carol Nelson-Williams**[4,5], **Alfred A. Vichot**[4,5], **Sheng Chih Jin**[4], **Erin Loring**[4,5,6], **Verena Untiet**[3], **Taekyeong Yoo**[7], **Jungmin Choi**[4,5], **Shengxin Xu**[8], **Aihua Wu**[8], **Marieluise Kirchner**[9], **Philipp Mertins**[9], **Lars C. Rump**[1], **Ali Mirza Onder**[10], **Cory Gamble**[11], **Daniel McKenney**[12], **Robert W. Lash**[13], **Deborah P. Jones**[14], **Gary Chune**[15], **Priscila Gagliardi**[16], **Murim Choi**[7], **Richard Gordon**[8], **Michael Stowasser**[8], **Christoph Fahlke**[3], and **Richard P. Lifton**[4,5,6,17]

[1]Department of Nephrology, Medical School, Heinrich Heine University Düsseldorf, 40225 Düsseldorf, Germany

[2]Department of Nephrology and Medical Intensive Care, Charité - Universitätsmedizin Berlin, Berlin Institute of Health, 10117 Berlin, Germany

[3]Institute of Complex Systems, Zelluläre Biophysik (ICS-4), Forschungszentrum Jülich, 52425 Jülich, Germany

[4]Department of Genetics, Yale University School of Medicine, New Haven, CT 06510, USA

[5]Howard Hughes Medical Institute, Yale University School of Medicine, New Haven, CT 06510, USA

[6]Yale Center for Mendelian Genomics, New Haven, CT 06510, USA

[*]*Correspondence and material requests should be addressed to:* Ute I. Scholl, M.D., BIH Johanna Quandt Professorship for Hypertension and Molecular Biology of Endocrine Tumors, Department of Nephrology and Medical Intensive Care, Charité – Universitätsmedizin Berlin and Berlin Institute of Health, Charitéplatz 1, 10117 Berlin, Germany. Telephone: +49-30-450-543080, Fax +49-211-81-015-04086, ute.scholl@charite.de.

[#]These authors contributed equally.

URLs

ClinVar, https://www.ncbi.nlm.nih.gov/clinvar/; github, https://github.com/murim76/gene_burden_test/blob/master/Compare_VCF_for_Scholl.pl; GEO series accession, https://www.ncbi.nlm.nih.gov/geo/query/acc.cgi?acc=GSE107030; The Human Protein Atlas, http://www.proteinatlas.org/ENSG00000165478-HEPACAM/cell/HEK+293, retrieved on 06/27/2017; FastQC, https://www.bioinformatics.babraham.ac.uk/projects/fastqc/; GTEx Portal, http://www.gtexportal.org/home/gene/HEPACAM.

Author Contributions

UIS, GS, ChF, and RPL designed the study. MS and RG recruited and characterized Family 3. AMO, CG, DM, RWL, DPJ, GC, PG, EL, CNW, and RPL ascertained and recruited probands with early-onset primary aldosteronism. AAV, EL, and UIS recruited additional members of selected families. CNW, SX, and AW prepared DNA samples; UIS, AAV, SCJ, TY, MC, and RPL analyzed exome sequencing results; UIS identified the disease gene; CNW, AT, and AAV performed and analyzed targeted DNA sequencing; JS performed immunohistochemistry, immunoprecipitation and real-time PCR; JS and AT made constructs and generated stable cell lines; JS and JC prepared samples for and analyzed RNA sequencing; JS and UIS performed and analyzed splicing assay and confocal microscopy; GS, HT, VU and ChF performed and analyzed FLIM and electrophysiology; MK and PM performed and analyzed mass spectrometry; LCR read and revised the manuscript; UIS wrote the initial draft of the manuscript, with contributions and/or revisions from all authors.

Competing financial interests

Heinrich Heine University Düsseldorf has filed a patent application: EP17209972, Diagnosis and Therapy of Primary Aldosteronism.

[7]Department of Biomedical Sciences, Seoul National University College of Medicine, Seoul 03080, Republic of Korea

[8]Endocrine Hypertension Research Center, University of Queensland Diamantina Institute, Greenslopes and Princess Alexandra Hospitals, Brisbane, Australia

[9]Proteomics Platform, Max Delbrück Center for Molecular Medicine in the Helmholtz Society and Core Unit Proteomics, Berlin Institute of Health, 13125 Berlin, Germany

[10]Le Bonheur Children's Hospital, Memphis, TN 38105, USA

[12]Cooper Clinic, PA, Fort Smith, AR 72903, USA

[12]Peyton Manning Children's Hospital at St. Vincent, Indianapolis, IN 46260, USA

[13]Division of Metabolism, Endocrinology, and Diabetes, University of Michigan Medical School, Ann Arbor, MI 48109, USA

[14]Division of Nephrology and Hypertension, Department of Pediatrics, Vanderbilt University School of Medicine, Nashville, TN 37232, USA

[15]Olin Teague Veterans Administration Hospital, Temple, TX 76504, USA

[16]Division of Endocrinology, Nemours Children's Specialty Care, Jacksonville, FL 32207, USA

[17]Laboratory of Human Genetics and Genomics, The Rockefeller University, New York, NY 10065, USA

Abstract

Primary aldosteronism, a common cause of severe hypertension[1], features constitutive production of the adrenal steroid aldosterone. We analyzed a multiplex family with familial hyperaldosteronism type II (FH-II)[2] and 80 additional probands with unsolved early-onset primary aldosteronism. Eight probands had novel heterozygous variants in *CLCN2*, including two *de novo* mutations and four independent occurrences of the identical p.Arg172Gln mutation; all relatives with early-onset primary aldosteronism carried the *CLCN2* variant found in probands. *CLCN2* encodes a voltage-gated chloride channel expressed in adrenal glomerulosa that opens at hyperpolarized membrane potentials. Channel opening depolarizes glomerulosa cells and induces expression of aldosterone synthase, the rate-limiting enzyme for aldosterone biosynthesis. Mutant channels cause gain of function, with higher open probabilities at the glomerulosa resting potential. These findings for the first time demonstrate a role of anion channels in glomerulosa membrane potential determination, aldosterone production and hypertension. They establish the cause of a substantial fraction of early-onset primary aldosteronism.

More than 1.1 billion people worldwide have hypertension[3], the single largest cause of premature mortality[4]. About 6% of hypertensive patients in primary care have primary aldosteronism[1], with higher frequencies among patients with severe hypertension. The plasma aldosterone level in primary aldosteronism is constitutively elevated despite low levels of the normal upstream regulator renin; hypokalemia is variable. Aldosterone-producing adrenal adenomas (APAs) and idiopathic hyperaldosteronism[5] are common causes of primary aldosteronism. Somatic mutations in *KCNJ5, CACNA1D, ATP1A1*, or

ATP2B3 that cause increased glomerulosa cell Ca^{2+} are sufficient for producing APAs[6–10]; germline mutations alter *CYP11B2*[11] in glucocorticoid-remediable aldosteronism (GRA, FH-I), *KCNJ5*[6,12] in FH-III, *CACNA1H*[13] in FH-IV, and *CACNA1D*[7] in PASNA syndrome[14]. These mutations define a common pathway for induction of aldosterone biosynthesis – glomerulosa cell membrane depolarization activates voltage-gated Ca^{2+} channels, which induces the rate-limiting enzyme for aldosterone biosynthesis, aldosterone synthase (*CYP11B2*), along with other enzymes in the biosynthetic pathway; increased mitochondrial Ca^{2+} may also contribute[15].

In 1992, Stowasser et al. described a multiplex kindred featuring autosomal dominant primary aldosteronism that was clinically distinct from GRA, the only dominant syndrome then known, and hence called it FH-II[2]. The responsible gene in this kindred has not been identified. We recruited an additional affected individual of this kindred[2,16] (family 3, Fig. 1, Table 1, Supplementary Note) and performed exome sequencing[13] of three affected subjects, revealing two shared novel protein-changing heterozygous variants in *CLCN2* (p.Arg172Gln, NP_004357) and *LINGO1* (p.His591Gln, NP_116197) (Supplementary Table 1). *CLCN2* was considered the more likely candidate gene based on conservation (Fig. 1), expression levels in human adrenal cortex (8.14 for *CLCN2*, 5.91 for *LINGO1*, log2 scale, mean expression of all genes 7.20[6]), and segregation analysis in the pedigree (Supplementary Table 2, Fig. 1).

We next searched for rare (allele frequency $<10^{-5}$ in public databases) damaging[17] variants in *CLCN2* and *LINGO1* among the exomes of 35 unrelated individuals diagnosed with unsolved primary aldosteronism by age 10 years – an extreme phenotype[13]. Only *CLCN2* showed such variants. All four were heterozygous and absent in public databases (Supplementary Table 1). Remarkably, one proband had the identical p.Arg172Gln variant found in family 3. In three additional subjects, p.Met22Lys and p.Tyr26Asn occurred at positions conserved through invertebrates, and one variant produced a new splice donor site resulting in an in-frame deletion (p.Lys362del) (Fig. 1, see below).

Analysis of *CLCN2* in 45 additional unrelated subjects diagnosed with primary aldosteronism by age 20 years (Supplementary Table 3) revealed two additional occurrences of p.Arg172Gln (Fig. 1). Additionally, p.Ser865Arg occurred at a moderately conserved position (Fig. 1). Sanger sequencing confirmed all variants (Supplementary Fig. 1). Sequencing of Arg172 in 1587 additional subjects referred for potential Mendelian hypertension, including 375 with primary aldosteronism diagnosed after age 20, identified no p.Arg172Gln variants, supporting enrichment in early-onset primary aldosteronism.

Among the four kindreds with p.Arg172Gln, one mutation (in kindred 318) occurred *de novo* (absent in proband's biological parents; Fig. 1, Supplementary Table 4). Among the other three kindreds, the maximum lengths of shared mutation-linked haplotypes between pairs of individuals ranged from 4,894 bp to 357,885 bp (Supplementary Table 5), with the putative last shared ancestor occurring ~651 (95% CI, 203–2615) to ~50,000 generations ago (95% CI, 10,000–infinity)[18]. While extremely remote common ancestry is a possibility, independent occurrence is overwhelmingly likely. After finding this mutation in the first family, the probability of finding, by chance, three additional independent instances of

p.Arg172Gln (one *de novo*), among 80 probands is 6.5×10^{-12} (Online Methods). The probability of any pair of these variants being identical by descent from a remote common ancestor is even lower. Lastly, the burden of rare protein-altering *CLCN2* variants in primary aldosteronism kindreds is significantly higher than in controls (8/81 vs. 6/3578, $p=1.3\times10^{-10}$, relative risk 58.9, Supplementary Table 6).

Sanger sequencing identified eight carriers of the p.Arg172Gln variant in family 3 (Fig. 1, Supplementary Fig. 1, Table 1, Supplementary Note). Seven carriers had elevated aldosterone/renin ratios (ARRs, a screening test for primary aldosteronism); those tested had positive confirmatory fludrocortisone suppression tests (FSTs) and non-lateralizing aldosterone production. One subject had repeatedly normal ARRs, suggesting incomplete penetrance. Subject 3-1, diagnosed with hypertension in her 30s and with primary aldosteronism at age 66 years, was *CLCN2* wildtype (Supplementary Table 2). In addition to later onset, she was distinct in having increased aldosterone with upright posture, typical of sporadic idiopathic hyperaldosteronism[5]. In kindred 1786, the proband's affected mother and brother carried the p.Arg172Gln variant. The brother had borderline ARR with suppressed renin and prehypertension at age 13 years. Subject 1492-1 was diagnosed with hypertension and primary aldosteronism in infancy, but became normotensive by age 2, suggesting variable expressivity with age. Among other probands, the p.Met22Lys variant was *de novo* (Supplementary Table 4). Thus in two of the four kindreds with parental data, rare *CLCN2* mutations were *de novo*.

In silico splice site analysis[19] of the variant in kindred 1492 predicted the creation of a new splice donor at the end of exon 10, three base pairs upstream of the normal splice donor. In a splicing assay in HEK cells (Supplementary Note), the wildtype exon was normally spliced, but the mutation resulted exclusively in splicing at the predicted upstream site, producing an in-frame deletion of codon 362 (Supplementary Fig. 1).

ClC-2, the chloride channel encoded by *CLCN2*, is found in many tissues, including brain, kidney, lung, and intestine[20]. Additionally, *CLCN2* RNA is found in the adrenal gland (see above). Immunohistochemistry with an antibody specific for ClC-2 revealed intense staining of human adrenal zona glomerulosa (Fig. 2, Supplementary Fig. 2), consistent with a role in regulating aldosterone production.

Chloride channels can conduct excitatory (membrane depolarizing) chloride efflux or inhibitory influx, depending on the ratio of chloride concentration on either side of the cell membrane. We determined the intracellular chloride concentration ($[Cl^-]_{int}$) in mouse adrenal gland slices (Fig. 3a,b, Supplementary Fig. 2) using fluorescence lifetime imaging microscopy; the method is based on the concentration-dependent fluorescence quenching of a chloride-sensitive dye[21]. The median value of $[Cl^-]_{int}$ was 74.7 mM. The distribution of intracellular glomerulosa chloride concentrations is rather broad, as expected for a dynamic equilibrium in cells with oscillating membrane potentials[22]. With a normal plasma Cl^- concentration of 100 mM, the calculated chloride reversal potential at 37°C is −8 mV, predicting that opening of ClC-2 in glomerulosa cells will result in chloride efflux and depolarization from the resting potential of about −80 mV[22]. This depolarization is predicted to activate voltage-gated Ca^{2+} channels, inducing aldosterone biosynthesis.

A facultative subunit of ClC-2 in glia, GlialCAM/HEPACAM[23], is not expressed in human adrenal gland (GTEx portal, see URLs). We therefore expressed wildtype (ClC-2^{WT}) and each of the mutant ClC-2s (ClC-2^{MUT}) alone in HEK293T cells and performed whole-cell patch clamp electrophysiology at $[Cl^-]_{int}$=75 mM. ClC-2^{WT} channels are closed at depolarized voltages and activate slowly at voltages negative to the chloride reversal potential[20,24,25]. All mutants shifted the activation curve to more positive voltages (Fig. 3, Supplementary Fig. 3, Supplementary Table 8). CLC channels are homodimers, with each subunit forming a separate conduction pathway. Each protopore can be individually opened and closed by a fast protopore gate, and a common slow gating mechanism acts on both pores[24,26]. Whereas p.Ser865Arg slowed down deactivaton of both gates and altered the protopore open probability, all other variants modified the common gate by increasing its minimum open probability and accelerating its activation (Fig. 3 and Supplementary Fig. 3). Mass spectrometry demonstrated that p.Ser865 was phosphorylated, suggesting a regulatory mechanism (Supplementary Fig. 4). The observed gating alterations with ClC-2^{MUT} predict significantly larger chloride efflux versus ClC-2^{WT} in glomerulosa cells at physiological membrane potentials.

To characterize the impact of ClC-2^{WT} and ClC-2^{MUT} in human adrenal glomerulosa cells, we expressed channels in human H295R adrenocortical cancer cells, an established model of aldosterone production[27]. Confocal microscopy revealed partial colocalization of YFP-tagged ClC-2^{WT} and ClC-2^{MUT} with a surface membrane marker; p.Met22Lys showed less colocalization than ClC-2^{WT} (Supplementary Fig. 4). RNA-Seq (Fig. 4a, Supplementary Table 9) demonstrated that transfection of untagged WT and p.Arg172Gln *CLCN2* both significantly increased expression of *CYP11B2* and its upstream regulator *NR4A2* (*NURR1*)[28]; *RGS4*, which provides feedback inhibition of Ang II-triggered signaling[29], was also upregulated. Quantitative real-time PCR of *CYP11B2* revealed that transfection of $CLCN2^{MUT}$ produced significantly greater increases in *CYP11B2* expression than $CLCN2^{WT}$ (Fig. 4b). In contrast, transfection of loss-of-function *CLCN2* mutations[30] did not change *CYP11B2* expression (Supplementary Fig. 5). H295R cells and their subclone HAC15 have negative membrane potentials[31]. Current-clamp recordings demonstrated significant depolarization of HAC15 upon WT *CLCN2* expression; p.Arg172Gln amplified this effect (Fig. 4c).

The finding of four independent occurrences of p.Arg172Gln (one *de novo*), along with four additional novel variants (one *de novo*) among 81 probands with early-onset primary aldosteronism provides strong evidence implicating these variants in disease pathogenesis. The localization of ClC-2 in adrenal zona glomerulosa is consistent with this observation. The electrophysiologic impact of mutant channels and their effect on aldosterone synthase expression demonstrate that these mutations cause gain of function, producing membrane depolarization and increasing *CYP11B2* expression (Fig. 4d). Because the syndrome in kindred 3 was named “FH-II”[2], we suggest to use this term for patients with germline *CLCN2* variants.

Retrospectively, efforts to map the disease gene in family 3[32] were challenged by a phenocopy (sporadic idiopathic hyperaldosteronism) in subject 3-1, incomplete penetrance and phenotypic uncertainty. Rare *CLCN2* variants explained primary aldosteronism in ~10%

of the early-onset cohort studied, suggesting there are likely additional genes yet undiscovered. Genetic testing for germline mutations in *CLCN2* and other early primary aldosteronism genes can be useful for establishing diagnosis, defining treatment options and assessing risk to future offspring.

Probands with FH-II showed early-onset primary aldosteronism and hypertension, often with hypokalemia. Hypertension was controlled with mineralocorticoid receptor antagonists or other antihypertensives (Supplementary Note). This phenotype appears indistinguishable from patients with *CACNA1H* mutations[13]. Hybrid steroid production and/or response to glucocorticoids, historically used to diagnose GRA[11], were absent, as were massive adrenal hyperplasia (present in many subjects with *KCNJ5* variants[6,12]) and neurodevelopmental abnormalities (characteristic of *CACNA1D* mutation[7]). Despite widespread *CLCN2* expression, subjects with gain-of-function *CLCN2* variants shared no apparent pathology other than primary aldosteronism, whereas loss-of-function *CLCN2* variants cause leukoencephalopathy with ataxia[33], with a similar phenotype in mice[34]. Incomplete penetrance or phenotypic amelioration with age, as sometimes occurs with germline mutations in *CYP11B2, KCNJ5, CACNA1D* and *CACNA1H*[7,12,13,35], occurred in some subjects with *CLCN2* mutations.

Our findings for the first time implicate activity of an anion channel in the regulation of aldosterone biosynthesis, primary aldosteronism and hypertension. Whether previously described slowly activating tiny chloride currents at strongly negative voltages in rat glomerulosa cells[15] or Ras-dependent chloride currents[36] represent ClC-2 is unclear. *In vivo*, ClC-2 may contribute to hyperpolarization-induced depolarization of adrenal glomerulosa cells, cyclic membrane potential oscillations, and aldosterone production[22]. Variants in primary aldosteronism would likely amplify these effects. Mouse models may prove useful to study such effects.

Online Methods

Subjects

Study subjects included the Australian kindred[2,32,37], 35 unrelated primary aldosteronism subjects without known disease-causing mutations, diagnosed by age 10 years (clinical characteristics published[13]), and 45 subjects diagnosed with primary aldosteronism by age 20 years (Supplementary Table 3). Selected families had additional members recruited. Controls were 3,578 unaffected parents of autistic offspring[38]. Research protocols were approved by local institutional review boards at Yale University and University of Queensland, and all probands and family members provided informed consent. Primary aldosteronism was diagnosed based on elevated aldosterone/renin ratio (ARR, >20 ng/dl:ng/ml/h or equivalent values)[5], with aldosterone >15 ng/dl, or marginally elevated values in the presence of hypokalemia. Confirmatory testing was performed according to the referring centers' guidelines[5]. Venous blood or saliva samples were obtained from subjects and family members and subjected to exome and/or Sanger sequencing[13].

DNA preparation and exome sequencing

DNA was prepared from venous blood or saliva samples using standard procedures. Exome capture was performed using the 2.1M NimbleGen Exome reagent (Roche NimbleGen, Madison, WI), and 75 base paired end sequencing on the Illumina (San Diego, CA) platform and analysis were performed as described[13].

Sanger sequencing of genomic DNA and genotyping of parent-offspring trios

Direct bidirectional Sanger sequencing of candidate variants from genomic DNA of indicated subjects was performed at Beckman Coulter Genomics (UK) or the Keck DNA sequencing facility at Yale University following PCR amplification. Rare variants identified in index cases through exome sequencing were genotyped by targeted PCR and Sanger sequencing in both parents to confirm paternity / maternity.

Immunohistochemistry and immunofluorescence

Formalin-fixed, paraffin-embedded 5 μm human adrenal gland sections were obtained from US Biomax (Rockville, MD, USA) and Pantomics (Richmond, CA, USA). Immunohistochemistry was performed as described[7], with the exception that 10% donkey serum was used for blocking. The concentration of the antigenic peptide was 0.4 mg/ml, and 1 μg peptide per μg antibody was used. Images were recorded on a Zeiss (Oberkochen, Germany) Axioplan 2 Imaging microscope (10× and 40× objectives) with a Zeiss AxioCam Mrc5 camera. Image cropping was performed in Adobe Illustrator CS4. Primary antibody against ClC-2 was HPA014545 (Sigma-Aldrich Prestige Antibodies, St. Louis, MO, USA; 1:100, incubation overnight at 4°C), and antibody against Dab2 was #sc-13982 (Santa Cruz, Santa Cruz, CA, USA; 1:100 dilution). Secondary antibody was donkey α-rabbit (#035-152, 1:200, Jackson, Bar Harbor, ME, USA, 2 h at room temperature) for human samples. To confirm the selection of the zona glomerulosa in mouse adrenal slices for fluorescence lifetime imaging (FLIM), slices were stained with the Dab2 antibody (1:100 dilution, incubation overnight at 4°C). Secondary antibody was donkey α-rabbit conjugated to Alexa Fluor 647 (A-31573, ThermoFisher Scientific; 1:1000, 2h at room temperature). Immunofluorescent images were recorded on a Leica TCS SP5 laser scanning confocal microscope (Leica Microsystems, Heidelberg, Germany).

Molecular cloning

Site directed mutagenesis (QuikChange, Agilent Technologies, Santa Clara, CA) was performed to introduce mutations into pcDNA5/FRT/TO ClC-2[24] according to the manufacturer's instructions. Primer sequences (M22K_F/_R, Y26N_F/_R, R172Q_F/_R, K362 del new_F/_R) are given in Supplementary Table 10. Each construct was validated by sequencing of the entire coding region. Mutant cDNAs were subcloned in frame into the pRcCMV vector containing the YFP cDNA using *NotI* and *PmlI* for use in confocal microscopy only. Two independent clones were assessed in all experiments (Supplementary Fig. 3).

Generation of stable cell lines

Stable HEK293 cell lines were generated using the Flp-In T-REx system (Invitrogen, Life Technologies, Carlsbad, CA, USA) according to the manufacturer's instructions. HEK293 cells do not express HEPACAM (Human Protein Atlas, see URLs). Flp-In T-REx 293 cells (authenticated, Eurofins Genomics) were cultured in high glucose DMEM (Biochrom GmbH, Berlin, Germany) with 10% FBS (Biochrom), 1% Penicillin/Streptomycin, 100 μg/mL Zeocin and 15μg/mL Blasticidin (all Invitrogen) at 37°C and 5% CO_2 humidified atmosphere. Cells were transfected with 2.4 μg pcDNA5/FRT/TO + insert (*CLCN2* mutants: p.Met22Lys, p.Tyr26Asn, p.Arg172Gln, p.Lys362del, p.Ser865Arg; two clones each) and 21.6 μg pOG44 using Lipofectamine 2000 (Invitrogen) and OPTIMEM (Gibco by Life Technologies, Carlsbad, CA, USA). The following day, the medium was changed to high glucose DMEM + 10% Tet-free FBS (Gibco) and 1% Penicillin/Streptomycin. 48 h after transfection, cells were split onto 15 cm dishes and selected with 15 μg/mL Blasticidin and 150 μg/mL Hygromycin (Invitrogen). Single colonies were selected. Variants were confirmed by Sanger sequencing of DNA extracted from stable cell lines, and inducible expression was verified by western blot (ClC-2 antibody #ACL-002, Alomone labs, Jerusalem, Israel).

The HAC15 cell line was kindly provided by Dr. William Rainey (University of Michigan), authenticated by short tandem repeat (STR) analysis (ATCC Cell Line Authentication Service) and cultured in DMEM/F12 (GlutaMAX; Gibco) + 5% HyClone Cosmic Calf Serum (CCS; GE Healthcare Life Sciences, Buckinghamshire, UK) +1% Penicillin-Streptomycin (Gibco) + 1% Insulin-Transferrin-Selenium (ITS; Gibco) +1% MEM Non-Essential Amino Acids Solution (Gibco) + 0.1% CD Lipid Concentrate (Gibco) at 37°C and 5% CO_2 in humidified atmosphere. Stable cell lines were prepared using the Piggybac transposon system (System Biosciences, Palo Alto, CA, USA). cDNAs of *CLCN2* (WT and Arg172Gln) were subcloned into pENTR-2B-Dual using NotI and XhoI. Gateway LR recombination (Invitrogen) was performed with pPiggybac-EF1 Neo + pTF rLTA (a kind gift of Dr. Celso Gomez-Sanchez, The University of Mississippi). Inserts were verified by Sanger sequencing. HAC15 cells were transfected using an Amaxa Nucleofector I (Lonza, Cologne, Germany; 2 million cells, 2 μg plasmid DNA, 0.8 μg Super Piggybac transposase; program X-005). After 48h, selection was initiated by addition of 5 μg/mL Blasticidin (Gibco) to the growth medium. Inducible expression was verified by western blot (ClC-2 antibody #ACL-002) after incubation with 1 μg/mL Doxycycline (Sigma Aldrich) for 24h.

Preparation of acute adrenal slices

After anesthetizing animals with isoflurane and decapitation, both adrenal glands were rapidly removed and placed in ice-cold Bicarbonate Buffered Saline (BBS) (125 mM NaCl, 2 mM KCl, 26 mM $NaHCO_3$, 0.1 mM $CaCl_2$, 5 mM $MgCl_2$, 10 mM glucose, constantly oxygenated with 5% CO_2 in O_2) for the removal of surrounding fat. The adrenal glands were embedded in 4% agarose in BBS, mounted, cut at 4°C (150–200 μm thick) with a Microm HM 650V (Thermo Scientific, Walldorf, Germany; frequency 60 Hz, amplitude 1 mm, drive 10) and held at 35°C for 30 min in BBS. Slices were subsequently stored in BBS at 37°C for further experiments. During each experiment, slices were constantly perfused with solution at 37°C, and all measurements were completed within 8 h of organ removal.

Fluorescence lifetime imaging microscopy (FLIM)

Prior to chloride imaging experiments, adrenal slices were incubated in BBS containing 10 mM 1-(ethoxycarbonylmethyl)-6-methoxyquinolinium bromide (MQAE; Sigma-Aldrich, Munich, Germany[39]) for 45–60 min at room temperature. Slices were transferred to an imaging chamber, perfused with BBS solution containing 2 mM instead of 0.1 mM Ca^{2+}, and FLIM was performed as described[21]. The solution was perfused through a heating coil resulting in a temperature of 37°C in the perfusion chamber. Fluorescence was stimulated by two-photon excitation (λ_{exc} = 750 nm), MQAE fluorescence was filtered (short pass filter, 500 nm, λ_{obs} < 510 nm; Omega Optical, Brattleboro, VT), and mean fluorescence lifetimes were measured using multidimensional time-correlated single photon counting (TCSPC). TCSPC electronics (SPC-152; Becker & Hickl) and acquisition software were used for FLIM as described[40]. We recorded data of 12 slices from 5 different C57BL/6 mice (2 male, 3 female) of age 3 months or older.

For chloride concentration calibration, MQAE fluorescence lifetimes of preset $[Cl^-]$ were measured. Adrenal slices were incubated in HEPES-buffered solution (140 mM K^+, 10 mM Na^+, 10 mM HEPES, 10–80 mM Cl^-, 70–140 mM gluconate, adjusted to 310 mOsmol/L with K–gluconate and to pH 7.4 with KOH, 37°C) containing 10 μM nigericin (sodium salt; Sigma-Aldrich, Munich, Germany) and 10 μM tributyltin (chloride salt; Sigma-Aldrich)[21,40–42]. The inverse fluorescence lifetime ($1/\tau$) was plotted, and the calibration curve was fitted as described before[21]. The Stern-Volmer constant (K_{SV} = 3.96) was determined as the product of τ_0 and the slope of the calibration curve. Since the fluorescence lifetime of MQAE is reduced by chloride via collisional quenching, MQAE fluorescence lifetimes and $[Cl^-]$ show a linear relationship:

$$\frac{\tau_0}{\tau} = 1 + K_{SV}[Cl^-]$$

Zona glomerulosa $[Cl^-]_{int}$ could then be calculated according to this relationship.

The three outermost cell layers were assumed to form the zona glomerulosa based on their characteristic nucleus to cytoplasm ratio and the corresponding staining with anti-DAB2 (#sc-13982, Santa Cruz) performed separately. Each cell was defined as a region of interest (ROI) with the exclusion of the nucleus, and fluorescence lifetimes were determined as mean values of the average fluorescence lifetimes of all pixels in a given ROI. Fluorescence lifetimes were calculated using SPCImage 5.6 (Becker&Hickl, Berlin, Germany) and exported for further extraction in Fiji. Statistics were performed using SigmaPlot 12 (Systat) and Python 3.5.2 + numpy 1.12.1 + scipy 0.18.1 + pandas 0.19.2 + seaborn 0.7.1 using built-in functions. The FLIM datasets generated during or analyzed during the current study are available on request. Python scripts for analysis are based on built-in functions of the above mentioned packages but are available on request.

Electrophysiological recordings

Flp-In T-REx stable cell lines were used for electrophysiological recordings. For each construct, at least two clones using at least two separate preparations were included in the

analysis. To avoid chloride depletion at large current amplitudes[24], Flp-In T-REx cells were used without induction. Whole-cell patch clamp currents were recorded on an EPC10 amplifier using PatchMaster software (both HEKA, Lambrecht/Pfalz, Germany). Borosilicate glass pipettes with open resistances between 0.9 and 2.5 MΩ were used. The extracellular solution for whole-cell recordings contained (in mM): NaCl (140), KCl (4), $CaCl_2$ (2), $MgCl_2$ (1) and HEPES (10) at pH 7.4. The intracellular solution contained (in mM): NaCl (73), $MgCl_2$ (1), NaGluconate (42), EGTA (5), HEPES (10) and MgATP (1) at pH 7.4. The liquid junction potential was calculated to be 1.9 mV and corrected for *a priori*. Cells were held at the calculated chloride reversal potential of −17.5 mV at rest.

Instantaneous current amplitudes at the fixed tail step to +60 mV were normalized and plotted against the preceding voltage step to reveal relative open probability curves. The durations of the voltage steps were 5 s for ClC-2^{WT} and ClC-$2^{Ser865Arg}$ and 1 s for all other mutations so that steady-state open probabilities were determined. Open probabilities (P_{open}) were fitted using a modified Boltzmann equation:

$$P_{\mathrm{open}}(V)=\frac{1}{1+e^{\frac{-(V-V_{1/2})}{k}}}$$

to allow for a comparison of the half-maximal activation($V_{1/2}$).

Fitting of the activation and deactivation current traces with the sum of two exponential functions revealed fast (τ_1) and slow (τ_2) time constants, respectively:

$$I(t)=A_0+A_1\cdot e^{-\frac{t}{\tau_1}}+A_2\cdot e^{\frac{-t}{\tau_2}}$$

CLC chloride channels are double-barreled channels with two conduction pathways. Protopores can be individually opened and closed by a fast gating process, but also jointly by slow common gating. Under the assumption that protopore and common gating processes are independent, the overall open probability equals the product of the respective individual open probabilities[43]:

$$P_{\mathrm{open}}=P_{\mathrm{fast}}\cdot P_{\mathrm{slow}}$$

By inserting a 15 ms pulse to −220 mV between the variable test pulse and the tail pulse, the ClC-2 fast gate is maximally opened (P_{fast} = 1)[44], and the common gate open probability can be determined. Fast protopore gate open probabilities were calculated by dividing the overall open probability by the common gate open probability.

Resting potentials in untransfected or in induced (1 μg tetracycline/ml medium for 24h) stably transfected HAC15 cells were measured using the perforated patch technique[45] in the current clamp mode. The extracellular solution contained (in mM): 140 NaCl, 10 HEPES, 4 KCl, 2 $CaCl_2$, 1 $MgCl_2$ adjusted to a pH of 7.4. The pipette solution contained (in mM): 130 KCl, 10 HEPES, 5 NaCl with the pH adjusted to 7.4. To maintain the native intracellular [Cl^-], we included the pore-forming, monovalent cation selective antibiotic gramicidin D

(Sigma-Aldrich) in the pipette solution to obtain access to the inside of the cell[45]. Gramicidin stock solution (50 mg/ml in DMSO) was prepared daily, and the diluted solution (final concentration: 100 μg/ml) was prepared every 2 h. The tip of the pipette (open resistance 1.5–3 MΩ) was filled with solution lacking gramicidin to facilitate gigaseal formation. Break-in was typically observed after 15–45 minutes. Resting potentials were determined using a HEKA EPC-10 patch clamp amplifier and the PatchMaster software (HEKA Elektronik) from the mean of 10–60 s long voltage recording segments with the current clamped to 0 pA. Only cells that exhibited ClC-2 like currents (visible slow activation upon hyperpolarization and a current larger than 40 pA at −160 mV in subsequent voltage-clamp experiments) were used for analysis.

Analysis of all electrophysiological experiments was performed using FitMaster software (HEKA Elektronik), SigmaPlot 12 (Systat) and Python 3.5.2 + numpy 1.12.1 + scipy 0.18.1 + pandas 0.19.2 using built-in functions. The electrophysiology datasets generated during or analyzed during the current study are available on request. Python scripts for analysis are based on built-in functions of the above mentioned packages but are available on request. Normality was assessed by Shapiro-Wilk test.

Culture of H295R cells

H295R human adrenocortical cells (a kind gift of Dr. Matthias Haase, Düsseldorf) were authenticated by short tandem repeat (STR) analysis (ATCC Cell Line Authentication Service) and cultured in DMEM/F12 + HEPES (Gibco) + 2.5 % Ultroser G (Pall, Port Washington, NY, USA) + 1% Insulin-Transferrin-Selenium+ (ITS+; Corning, Corning, NY, USA) + 1 % Penicillin/Streptomycin (Gibco) at 37°C and 5% CO_2 in humidified atmosphere.

Quantitative real-time PCR

Three million H295R cells were resuspended in 100 μl Nucleofector solution R (Lonza) plus 3 μg plasmid DNA (pcDNA/FRT/TO empty vector, WT or mutant *CLCN2*) and electroporated with program P-20 using an Amaxa Nucleofector I (Lonza). After recovering of the cells in RPMI 1640 medium (Gibco) for 15 min at 37°C, they were plated on 12-well plates. 24h after transfection, H295R cells were starved in DMEM/F12 + HEPES + 0.1 % Ultroser G + 1 % Penicillin/Streptomycin for additional 24h. Total RNA was isolated using the RNeasy® Mini Kit (Qiagen GmbH, Hilden, Germany) and quantified with a Nanodrop 2000 (Thermo Scientific, Wilmington, DE, USA). After reverse transcription of RNA using Quantitect RT Kit (Qiagen), Taqman gene expression assays (Applied Biosystems, Foster City, CA, USA) for *GAPDH* (HS02758991_g1) as housekeeping gene and *CYP11B2* (Hs01597732_m1) as gene of interest were performed using the Taqman Gene Expression Master Mix. Each variant was assessed in parallel with wildtype and empty vector control. Gene expression was evaluated relative to the housekeeping gene and expressed as $2^{\Delta\Delta Ct}$. Normality was assessed by Shapiro-Wilk test. Statistical differences were assessed by ratio-paired two-tailed t tests (for normally distributed individual data), one-way ANOVA (for normally distributed multiple comparisons; adjusted p value reported) or Friedman test (multiple comparisons, no normal distribution; adjusted p value reported) in Graphpad Prism 7.

Whole-transcriptome sequencing, read alignment and differential gene expression analysis

H295R cells were transfected in two independent reactions as above, RNA was isolated using Trizol (Thermo Fisher Scientific), followed by DNase digest and column purification (RNeasy, Qiagen). Libraries were prepared after Poly A selection. Samples were sequenced on the Illumina HiSeq2500 at the Yale Center for Genome Analysis, producing a mean of 47.9 million 75-bp single-end reads. The quality of the raw sequencing reads was evaluated using FastQC version 0.10.4 (see URLs), and the base of lower quality (base quality score < 20) in the last position was trimmed. Tophat v2.1.1[46] was used to align the high quality sequencing reads to the reference human genome sequence build hg19. Differentially expressed genes were identified by Cuffdiff v2.2.1[47]. An FDR adjusted p value (q value) ≤ 0.05 and $|\log_2(\text{Fold Change})| \geq 1$ were set as the cutoffs for significantly differential expression.

Estimation of the probability of observing one *de novo* and two transmitted p.Arg172Gln variants in *CLCN2*

From the identification of the novel p.Arg172Gln variant in family 3, we calculated the probability of finding an identical *de novo* mutation and two independent instances of the same transmitted variant by chance among 80 probands. Using the genome-wide mutation rate of 1.67×10^{-8} per base per generation from a recent study[48], we estimated that the probability of seeing any specific *de novo* mutation in one individual is 3.34×10^{-8}. For transmitted events, we applied the UnseenEst[49] algorithm to estimate the probability of finding an unseen missense mutation in human populations. A total of 33,778 healthy individuals were selected from the ExAC database[50] to match the population distribution of the 2,010 U.S. Census. The U.S. Census-matched dataset was trained in the UnseenEst[49] algorithm to estimate the frequency distribution of distinct unseen missense mutations for the US population. The predicted frequency distribution was used to extrapolate the probability of observing one unseen transmitted event (probability = 2.81×10^{-5}). Taken together, the probability of observing one *de novo* and two transmitted p.Arg172Gln mutations among 80 independent samples is estimated to be

$$\binom{80}{2}\times(2.81\times10^{-5})^{2}\times(1-2.81\times10^{-5})^{78}\times\binom{78}{1}\times(3.34\times10^{-8})^{1}\times(1-\ 3.34\times10^{-8})^{77}=6.49\times10^{-12}.$$

Shared haplotypes and estimation of the mutation age of p.Arg172Gln in *CLCN2*

Genotypes of SNPs flanking the $CLCN2^{Arg172Gln}$ mutation were extracted from exome data. To estimate the mutation age of the *CLCN2* p.Arg172Gln mutation testing the assumption that the mutation is identical by descent among each possible pair of kindreds with the variant (except the documented *de novo* mutation), we used the ESTIAGE algorithm to estimate the pairwise time of coalescence for the three pairs of kindreds as previously described[13,18]. ESTIAGE uses a maximum-likelihood approach to estimate the mutation age, which takes into account the frequencies of the shared allele at each marker and the recombination fractions between the mutation of interest and polymorphic markers located within or at the boundaries of the shared haplotype. Seventeen polymorphic markers

spanning the shared haplotype were used for input (Supplementary Table 5). The marker allele frequencies were estimated from the Finnish and Non-Finnish European populations in the ExAC database[50], and the mutation rate was set to 2×10^{-8}.

Statistics

The statistical analyses used throughout the manuscript are described in the corresponding results and Online Methods paragraphs, Figure legends or Supplementary Tables.

Data availability

CLCN2 variants are deposited in ClinVar (accession numbers SCV000606833-7), RNAseq data are at GEO (accession number GSE107030, see URLs).

Code availability

Code for gene burden analysis is available at github (see URLs).

Supplementary Material

Refer to Web version on PubMed Central for supplementary material.

Acknowledgments

We thank our patients and their families for their invaluable contributions, the Yale Center for Genome Analysis for next-generation sequencing, the Center for Advanced Imaging (CAi) at Heinrich Heine University for providing a confocal microscope, Stefanie Weidtkamp-Peters and Sebastian Hänsch for technical assistance, Junhui Zhang for helpful discussions, Eric Seidel, Nadine Erlenhardt and Nicolai Klöcker for providing immunoprecipitation protocols and helpful discussions, Celso Gomez-Sanchez (The University of Mississippi) for providing plasmids, William Rainey (University of Michigan) for providing HAC15 cells and Matthias Haase (Heinrich Heine University Düsseldorf) for providing H295R cells. Computational support and infrastructure were in part provided by the Centre for Information and Media Technology (Düsseldorf). Supported in part by the Ministerium für Kultur und Wissenschaft des Landes Nordrhein-Westfalen (Rückkehrprogramm and Junges Kolleg), the Deutsche Forschungsgemeinschaft (SCHO 1386/2-1) (all UIS), the NIH Center for Mendelian Genomics (5U54HG006504), NIH P01DK17433, and the Howard Hughes Medical Institute (all RPL).

References

1. Monticone S, et al. Prevalence and Clinical Manifestations of Primary Aldosteronism Encountered in Primary Care Practice. J Am Coll Cardiol. 2017; 69:1811–1820. [PubMed: 28385310]
2. Stowasser M, et al. Familial hyperaldosteronism type II: five families with a new variety of primary aldosteronism. Clin Exp Pharmacol Physiol. 1992; 19:319–22. [PubMed: 1521363]
3. Collaboration, N.C.D.R.F. Worldwide trends in blood pressure from 1975 to 2015: a pooled analysis of 1479 population-based measurement studies with 19.1 million participants. Lancet. 2016
4. Lim SS, et al. A comparative risk assessment of burden of disease and injury attributable to 67 risk factors and risk factor clusters in 21 regions, 1990–2010: a systematic analysis for the Global Burden of Disease Study 2010. Lancet. 2012; 380:2224–60. [PubMed: 23245609]
5. Funder JW, et al. The Management of Primary Aldosteronism: Case Detection, Diagnosis, and Treatment: An Endocrine Society Clinical Practice Guideline. J Clin Endocrinol Metab. 2016; 101:1889–916. [PubMed: 26934393]
6. Choi M, et al. K+ channel mutations in adrenal aldosterone-producing adenomas and hereditary hypertension. Science. 2011; 331:768–72. [PubMed: 21311022]
7. Scholl UI, et al. Somatic and germline CACNA1D calcium channel mutations in aldosterone-producing adenomas and primary aldosteronism. Nat Genet. 2013; 45:1050–4. [PubMed: 23913001]

8. Azizan EA, et al. Somatic mutations in ATP1A1 and CACNA1D underlie a common subtype of adrenal hypertension. Nat Genet. 2013; 45:1055–60. [PubMed: 23913004]
9. Beuschlein F, et al. Somatic mutations in ATP1A1 and ATP2B3 lead to aldosterone-producing adenomas and secondary hypertension. Nat Genet. 2013; 45:440–4. [PubMed: 23416519]
10. Fernandes-Rosa FL, et al. Genetic spectrum and clinical correlates of somatic mutations in aldosterone-producing adenoma. Hypertension. 2014; 64:354–61. [PubMed: 24866132]
11. Lifton RP, et al. A chimaeric 11 beta-hydroxylase/aldosterone synthase gene causes glucocorticoid-remediable aldosteronism and human hypertension. Nature. 1992; 355:262–5. [PubMed: 1731223]
12. Scholl UI, et al. Hypertension with or without adrenal hyperplasia due to different inherited mutations in the potassium channel KCNJ5. Proc Natl Acad Sci U S A. 2012; 109:2533–8. [PubMed: 22308486]
13. Scholl UI, et al. Recurrent gain of function mutation in calcium channel CACNA1H causes early-onset hypertension with primary aldosteronism. Elife. 2015; 4
14. Korah HE, Scholl UI. An Update on Familial Hyperaldosteronism. Horm Metab Res. 2015; 47:941–6. [PubMed: 26445452]
15. Spat A, Hunyady L. Control of aldosterone secretion: a model for convergence in cellular signaling pathways. Physiol Rev. 2004; 84:489–539. [PubMed: 15044681]
16. Carss KJ, Stowasser M, Gordon RD, O'Shaughnessy KM. Further study of chromosome 7p22 to identify the molecular basis of familial hyperaldosteronism type II. J Hum Hypertens. 2011; 25:560–4. [PubMed: 20927129]
17. Dong C, et al. Comparison and integration of deleteriousness prediction methods for nonsynonymous SNVs in whole exome sequencing studies. Hum Mol Genet. 2015; 24:2125–37. [PubMed: 25552646]
18. Genin E, Tullio-Pelet A, Begeot F, Lyonnet S, Abel L. Estimating the age of rare disease mutations: the example of Triple-A syndrome. J Med Genet. 2004; 41:445–9. [PubMed: 15173230]
19. Dogan RI, Getoor L, Wilbur WJ, Mount SM. SplicePort--an interactive splice-site analysis tool. Nucleic Acids Res. 2007; 35:W285–91. [PubMed: 17576680]
20. Thiemann A, Grunder S, Pusch M, Jentsch TJ. A chloride channel widely expressed in epithelial and non-epithelial cells. Nature. 1992; 356:57–60. [PubMed: 1311421]
21. Untiet V, et al. Glutamate transporter-associated anion channels adjust intracellular chloride concentrations during glial maturation. Glia. 2017; 65:388–400. [PubMed: 27859594]
22. Hu C, Rusin CG, Tan Z, Guagliardo NA, Barrett PQ. Zona glomerulosa cells of the mouse adrenal cortex are intrinsic electrical oscillators. J Clin Invest. 2012; 122:2046–53. [PubMed: 22546854]
23. Jeworutzki E, et al. GlialCAM, a protein defective in a leukodystrophy, serves as a ClC-2 Cl(−) channel auxiliary subunit. Neuron. 2012; 73:951–61. [PubMed: 22405205]
24. Stolting G, et al. Regulation of ClC-2 gating by intracellular ATP. Pflugers Arch. 2013; 465:1423–37. [PubMed: 23632988]
25. Niemeyer MI, Cid LP, Zuniga L, Catalan M, Sepulveda FV. A conserved pore-lining glutamate as a voltage- and chloride-dependent gate in the ClC-2 chloride channel. J Physiol. 2003; 553:873–9. [PubMed: 14617675]
26. Jentsch TJ. Discovery of CLC transport proteins: cloning, structure, function and pathophysiology. J Physiol. 2015; 593:4091–109. [PubMed: 25590607]
27. Rainey WE, Bird IM, Mason JI. The NCI-H295 cell line: a pluripotent model for human adrenocortical studies. Mol Cell Endocrinol. 1994; 100:45–50. [PubMed: 8056157]
28. Bassett MH, Suzuki T, Sasano H, White PC, Rainey WE. The orphan nuclear receptors NURR1 and NGFIB regulate adrenal aldosterone production. Mol Endocrinol. 2004; 18:279–90. [PubMed: 14645496]
29. Romero DG, et al. Regulators of G-protein signaling 4 in adrenal gland: localization, regulation, and role in aldosterone secretion. J Endocrinol. 2007; 194:429–40. [PubMed: 17641290]
30. Garcia-Olivares J, et al. Gating of human ClC-2 chloride channels and regulation by carboxy-terminal domains. J Physiol. 2008; 586:5325–36. [PubMed: 18801843]

31. Tauber P, et al. Cellular Pathophysiology of an Adrenal Adenoma-Associated Mutant of the Plasma Membrane Ca(2+)-ATPase ATP2B3. Endocrinology. 2016; 157:2489–99. [PubMed: 27035656]
32. Lafferty AR, et al. A novel genetic locus for low renin hypertension: familial hyperaldosteronism type II maps to chromosome 7 (7p22). J Med Genet. 2000; 37:831–5. [PubMed: 11073536]
33. Depienne C, et al. Brain white matter oedema due to ClC-2 chloride channel deficiency: an observational analytical study. Lancet Neurol. 2013; 12:659–68. [PubMed: 23707145]
34. Blanz J, et al. Leukoencephalopathy upon disruption of the chloride channel ClC-2. J Neurosci. 2007; 27:6581–9. [PubMed: 17567819]
35. Stowasser M, et al. Clinical, biochemical and genetic approaches to the detection of familial hyperaldosteronism type I. J Hypertens. 1995; 13:1610–3. [PubMed: 8903619]
36. Chorvatova A, Gendron L, Bilodeau L, Gallo-Payet N, Payet MD. A Ras-dependent chloride current activated by adrenocorticotropin in rat adrenal zona glomerulosa cells. Endocrinology. 2000; 141:684–92. [PubMed: 10650950]
37. Torpy DJ, et al. Familial hyperaldosteronism type II: description of a large kindred and exclusion of the aldosterone synthase (CYP11B2) gene. J Clin Endocrinol Metab. 1998; 83:3214–8. [PubMed: 9745430]
38. Krumm N, et al. Excess of rare, inherited truncating mutations in autism. Nat Genet. 2015; 47:582–8. [PubMed: 25961944]
39. Verkman AS. Development and biological applications of chloride-sensitive fluorescent indicators. Am J Physiol. 1990; 259:C375–88. [PubMed: 2205105]
40. Kaneko H, Putzier I, Frings S, Kaupp UB, Gensch T. Chloride accumulation in mammalian olfactory sensory neurons. J Neurosci. 2004; 24:7931–8. [PubMed: 15356206]
41. Bevensee MO, Apkon M, Boron WF. Intracellular pH regulation in cultured astrocytes from rat hippocampus. II. Electrogenic Na/HCO3 cotransport. J Gen Physiol. 1997; 110:467–83. [PubMed: 9379176]
42. Chao AC, Dix JA, Sellers MC, Verkman AS. Fluorescence measurement of chloride transport in monolayer cultured cells. Mechanisms of chloride transport in fibroblasts. Biophys J. 1989; 56:1071–81. [PubMed: 2482083]
43. Accardi A, Pusch M. Fast and slow gating relaxations in the muscle chloride channel CLC-1. J Gen Physiol. 2000; 116:433–44. [PubMed: 10962018]
44. de Santiago JA, Nehrke K, Arreola J. Quantitative analysis of the voltage-dependent gating of mouse parotid ClC-2 chloride channel. J Gen Physiol. 2005; 126:591–603. [PubMed: 16286506]
45. Rhee JS, Ebihara S, Akaike N. Gramicidin perforated patch-clamp technique reveals glycine-gated outward chloride current in dissociated nucleus solitarii neurons of the rat. J Neurophysiol. 1994; 72:1103–8. [PubMed: 7528790]
46. Kim D, et al. TopHat2: accurate alignment of transcriptomes in the presence of insertions, deletions and gene fusions. Genome Biol. 2013; 14:R36. [PubMed: 23618408]
47. Trapnell C, et al. Differential analysis of gene regulation at transcript resolution with RNA-seq. Nat Biotechnol. 2013; 31:46–53. [PubMed: 23222703]
48. Samocha KE, et al. A framework for the interpretation of de novo mutation in human disease. Nat Genet. 2014; 46:944–50. [PubMed: 25086666]
49. Zou J, et al. Quantifying unobserved protein-coding variants in human populations provides a roadmap for large-scale sequencing projects. Nat Commun. 2016; 7:13293. [PubMed: 27796292]
50. Lek M, et al. Analysis of protein-coding genetic variation in 60,706 humans. Nature. 2016; 536:285–91. [PubMed: 27535533]

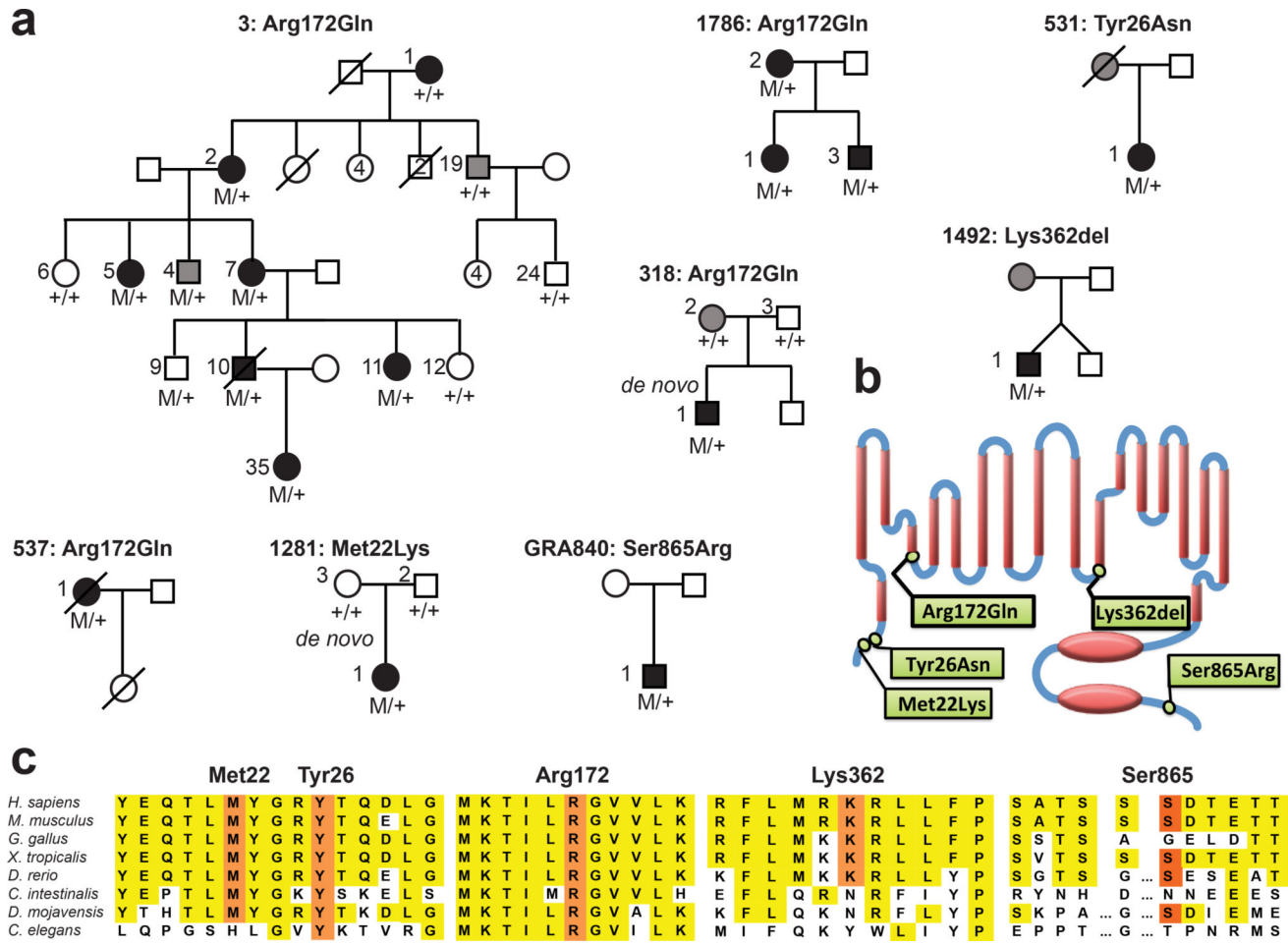

Figure 1. Kindreds with Hypertension and Primary Aldosteronism with *CLCN2* Mutations

(**a**) Pedigrees of eight kindreds with primary aldosteronism and hypertension, with indicated novel *CLCN2* variants. Filled black symbols denote subjects with primary aldosteronism, and filled grey symbols denote subjects with early-onset hypertension or borderline elevated ARRs. Genotypes are shown beneath each symbol, M/+ denotes the indicated novel *CLCN2* variant in the heterozygous state, and +/+ denotes homozygous wildtype sequence. (**b**) Position of the indicated variants in the N-terminus, D helix, K helix and C-terminus of the ClC-2 chloride channel encoded by *CLCN2*. Red ellipses represent C-terminal CBS domains. (**c**) Conservation of the respective amino acid positions among orthologous species (*H. sapiens*, human; *M. musculus*, mouse; *G. gallus*, chicken; *X. tropicalis*, western clawed frog; *D. rerio*, zebrafish; *C. intestinalis*, vase tunicate; *D. mojavensis*, fruit fly; *C. elegans*, roundworm).

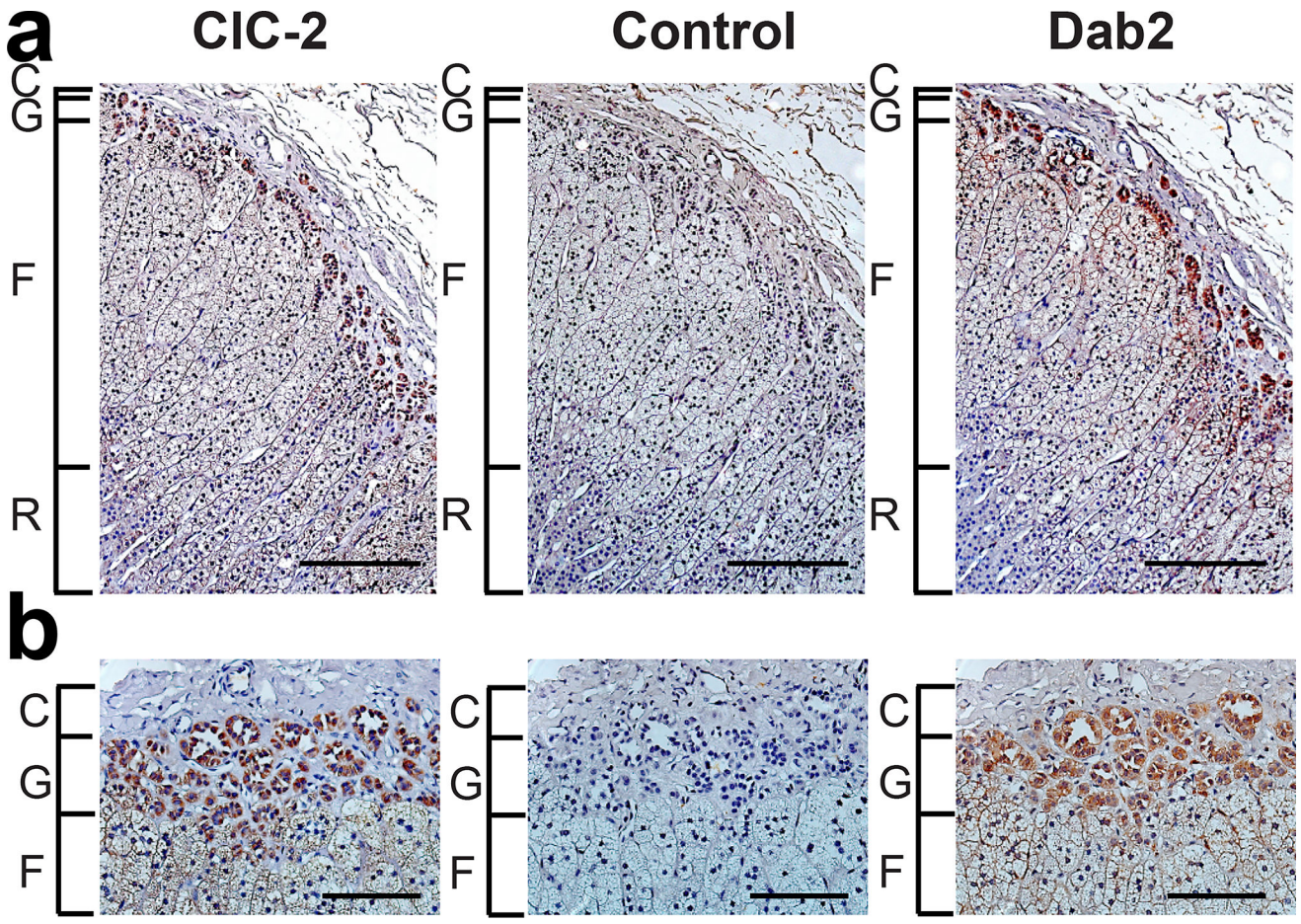

Figure 2. Expression of ClC-2 in Human Adrenal Gland

(**a**) Section of human adrenal cortex (C, capsule; G, glomerulosa; F, fasciculata; R, reticularis) stained by immunohistochemistry and counterstained with hematoxylin. One of two technical replicates is shown. Left, anti-ClC-2; middle, control preincubation of the anti-ClC-2 antibody with the antigenic peptide; right, anti-Dab2 as marker of the adrenal zona glomerulosa. The comparison of the three panels demonstrates specific expression of ClC-2, predominantly in the zona glomerulosa. Scale bars represent 200 μm. (**b**) Higher magnifications of the zona glomerulosa, scale bars represent 100 μm.

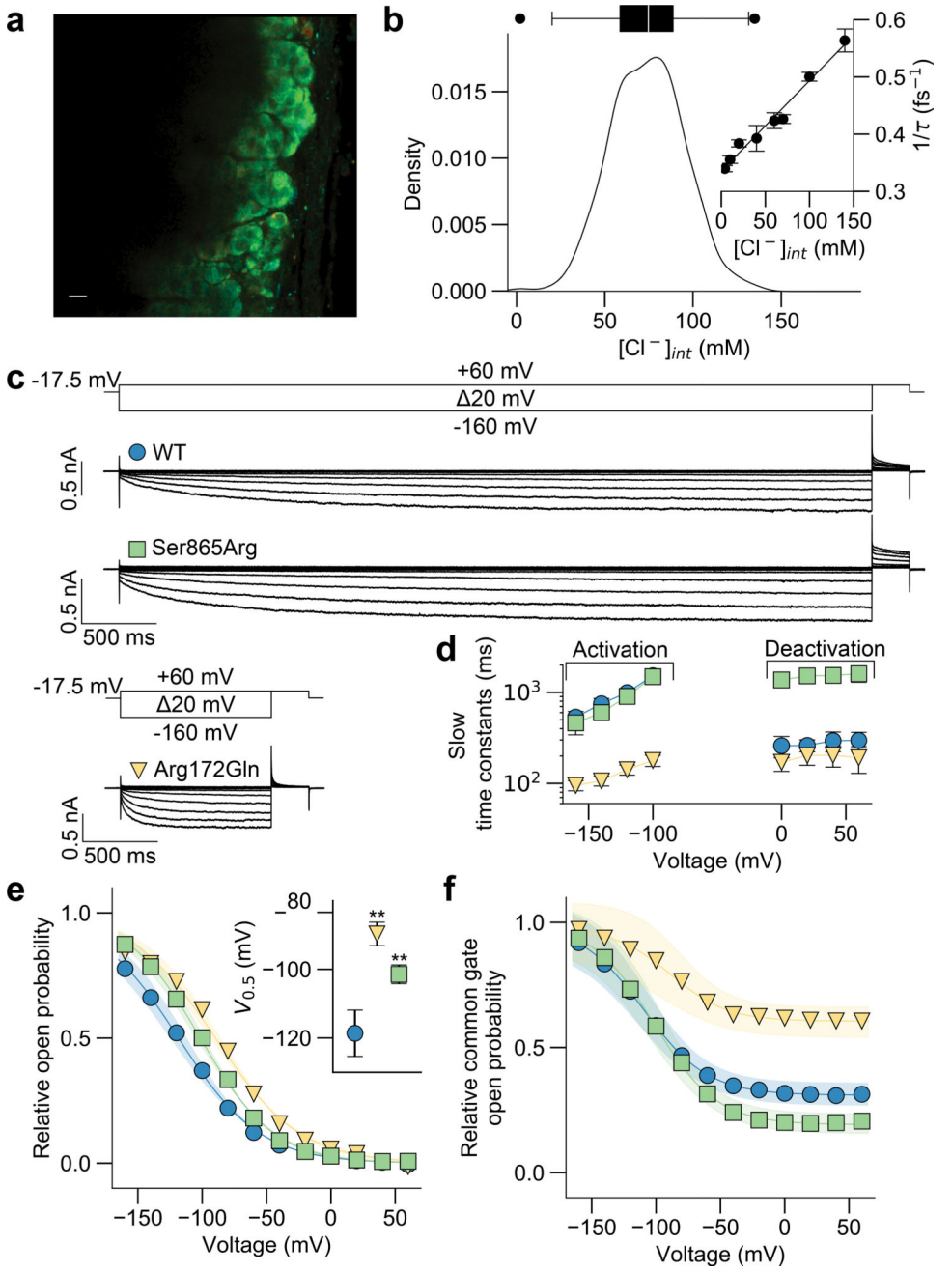

Figure 3. *CLCN2* Mutations Increase Excitatory Anion Efflux by Modifying the Voltage Dependence of Channel Opening

(**a**) Representative mouse adrenal gland section loaded with MQAE at 37°C. Short lifetimes (red, 1 ns) indicate high, long lifetimes (blue, 4 ns) low intracellular chloride concentrations. Scale bar, 10 μm. (**b**) Insert, calibration curve of MQAE fluorescence lifetimes in cells with preset intracellular chloride concentrations. A kernel density estimation of intracellular chloride concentrations for glomerulosa cells was obtained (Gaussian kernel, bandwidth=8.0 as determined by Scott's rule). Median intracellular chloride concentration was 74.7 mM (300 cells, 12 slices, five animals). Box, interquartile range; whiskers, 1.5× interquartile

range; line, median. **(c)** Whole-cell patch clamp recordings of representative ClC-2^{WT} and ClC-2^{MUT} and voltage protocol (150 mM $[Cl^-]_{out}$, 75 mM $[Cl^-]_{int}$, see Online Methods for solutions) are shown. **(d)** Time constants for representative ClC-2^{WT} and ClC-2^{MUT} with mean values ± 95% confidence intervals are shown (Supplementary Table 8). **(e)** and **(f)** Mean relative open probabilities (e) and common gate open probabilities (f) were fit with a Boltzmann function (bold lines, Supplementary Table 8) with 95% confidence intervals as calculated from a bootstrap resampling (translucent areas). Open probabilities of mutant channels are significantly higher at the glomerulosa resting potential of ~−80 mV (WT, 0.22±0.02 (n=11); p.Arg172Gln, 0.45±0.02 (n=13; $p<0.001$ vs. WT); p.Ser865Arg, 0.33±0.02 (n=12; $p<0.001$ vs. WT); all mean±SEM, one-way ANOVA; F=36.307; d.f.=5). The insert in (e) demonstrates the shift in voltage activation as assessed by the point of half maximal activation (Supplemental Table 8). **, $p<0.01$.

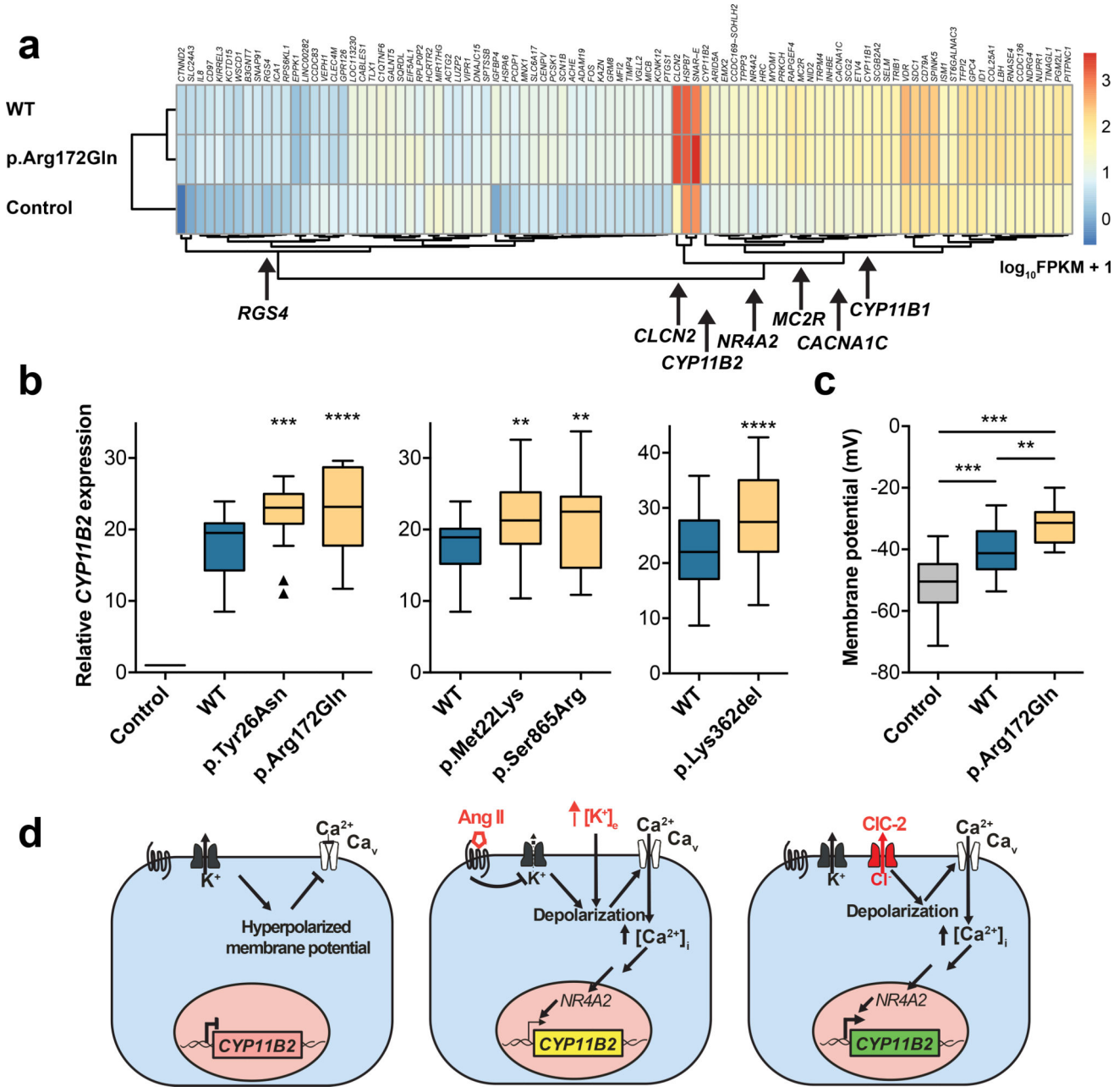

Figure 4. ClC-2 Increases Aldosterone Synthase Expression in H295R cells

(**a**) RNA sequencing of H295R cells transfected with *CLCN2* (WT or p.Arg172Gln), and vector control (heatmap). FPKM, fragments per kilobase of transcript per million fragments mapped. *CLCN2* and *CYP11B2* show the largest increase in expression versus control. Genes involved in adrenal function or calcium pathway are highlighted. (**b**) Relative expression levels of *CYP11B2* (box, interquartile range; whiskers, 1.5× interquartile range; line, median) in the H295R cell line after transfection with empty vector (control), $CLCN2^{WT}$ (blue), and $CLCN2^{MUT}$ (yellow). Parallel transfections and real-time PCRs were performed in each group. *CYP11B2* expression significantly increases after transfection of $CLCN2^{MUT}$ (see Supplementary Table 8 for statistical analysis). (**c**) Resting membrane

potential (plots as in b) of HAC15 cells stably expressing *CLCN2* (WT or p.Arg172Gln) and untransfected controls. WT and p.Arg172Gln cause significant depolarization versus control, and p.Arg172Gln causes significant depolarization versus WT (see Supplementary Table 8 for statistical analysis). (**d**) Model of ClC-2 function in human adrenal glomerulosa. Resting cells are hyperpolarized. Angiotensin II (AngII) and hyperkalemia cause depolarization, activation of voltage-dependent calcium channels, calcium influx, and increased *CYP11B2* expression via the transcription factor *NR4A2* (*NURR1*). ClC-2^{MUT} causes increased *CYP11B2* expression by membrane depolarization via increased Cl^- efflux. **, $p<0.01$; ***, $p<0.001$; ****, $p<0.0001$.

Table 1

Clinical Characteristics of Subjects with *CLCN2* Variants

Family ID	Subject ID	*CLCN2* variant	Gender	Age dx / blood draw	BP (mmHg)	BP %ile	K^+ (mM)	Aldo (ng/dl)	PRA (ng/ml/h)	ARR (ng/dl: ng/ml/h)
Normal range					**<140/90 in adults**	**<95th in children**	**3.5–5.5**			**< 20**
3	2	p.Arg172Gln	F	24	120/80 on 3 meds	NA	3.0	40.2	0.3	134.0
3	4	p.Arg172Gln	M	36	98/70 (age 24)	NA	4.2	24.5	1.2	20.4
3	5	p.Arg172Gln	F	19	150/100 on 1 med	NA	3.3	27.4	0.1	274.0
3	7	p.Arg172Gln	F	20	140/100	NA	3.8	26.5	0.1	265.0
3	9	p.Arg172Gln	M	18	120/80 (age 19)	NA	4.0	24.7	1.5	16.5
3	10	p.Arg172Gln	M	17	130/85	90–95th	4.0	26.2	0.1	262.0
3	11	p.Arg172Gln	F	14	94/62	≤ 50th	4.0	21.2	0.1	212.0
3	35	p.Arg172Gln	F	16	170/110	>99th	3.4	25.5	≤0.2	≥127.5
1786	1	p.Arg172Gln	F	15	150/100	>99th	2.9	47.9	<1.0	>47.9
1786	2	p.Arg172Gln	F	32	118/68 on 2 meds	NA	3.0	46.3	<1.0	>46.3
1786	3	p.Arg172Gln	M	13	121/75 (24 h)	>75th	4.4	12.0	<0.6	>20.0
537	1	p.Arg172Gln	F	11	160/120	>99th	3.0	26.0	0.3	86.7
318	1	p.Arg172Gln	M	7	170/140	>99th	2.6	9.5	0.21	45.2
1281	1	p.Met22Lys	F	1	117/71	>99th	4.1	17.0	<0.5	>34.0
531	1	p.Tyr26Asn	F	6	280/188 at age 20	NA	NA	100.0	<3.0	>33.3
840	1	p.Ser865Arg	M	15	130/100	90–95th/>99th	3.2	37.0	0.2	185.0
1492	1	p.Lys362del	M	0.2	150/90	>99th	4.0	63.8	<0.15	>425.3

Age dx, age at diagnosis; BP, blood pressure (office unless otherwise indicated); BP %ile, blood pressure percentile for subjects under age 18 years; K^+, serum potassium level; Aldo, serum aldosterone level; PRA, plasma renin activity; ARR, aldosterone/renin ratio. F, female; M, male; NA, not available or not applicable; med(s), antihypertensive medication(s). Reference values are given below each parameter.